Transversal Thermal Patterns in Packed-Bed Reactors with Simple Kinetics: Bifurcation Criterion and Simulations

Olga Nekhamkina and Moshe Sheintuch
Dept. of Chemical Engineering, Technion - I.I.T., Technion City, Haifa 32 000, Israel

DOI 10.1002/aic.12303
Published online July 2, 2010 in Wiley Online Library (wileyonlinelibrary.com).

We derive a new criterion for transversal instability of planar fronts based on the bifurcation condition $dV_f/dK|_{K=0} = 0$, where V_f and K are the front velocity and its curvature, respectively. This refines our previously obtained condition, which was formulated as $\alpha = (\Delta T_{ad} Pe_T)/(\Delta T_m Pe_C) > 1$ to $\alpha > 1 + |\delta|$, where ΔT_{ad} and ΔT_m are the adiabatic and maximal temperature rise, respectively, Pe_C and Pe_T are the axial mass and the heat Pe numbers, respectively, and δ is a small parameter. The criterion is based on approximate relations for ΔT_m and V_f, which account for the local curvature of a propagating front in a packed bed reactor with a first-order activated kinetics. The obtained relations are verified by linear stability analysis of planar fronts. Simulations of a simplified 2D model in the form of a thin cylindrical shell are in good agreement with the critical parameters predicted by dispersion relations. Three types of patterns were detected in simulations: "frozen" multiwave patterns, spinning waves, and complex rotating–oscillating patterns. We map bifurcation diagrams showing domains of different modes using the shell radius as the bifurcation parameter. The possible translation of the 2D cylindrical shell model results to the 3D case is discussed. © 2010 American Institute of Chemical Engineers *AIChE J,* 57: 735–748, 2011
Keywords: reactor analysis, simulation, process, fronts, bifurcations, transversal patterns

Introduction

Heterogeneous catalysts are extensively used in the chemical and petrochemical industry and for pollution abatement purposes. It is usually assumed that the temperature and concentrations of the reactants at any transversal cross section of an adiabatic packed-bed reactor are uniform. However, various industrial and laboratory experimental observations revealed formation of nonuniform temperature in the reactor cross section. Such patterns may pose severe safety hazards by altering the wall strength and inducing cracks. Ignoring such patterns in design and simulations may lead to erroneous results. Understanding which kinetics may lead to spatiotemporal pattern formation is essential for the development of design and control strategies that circumvent them.

Symmetry-breaking leading to either spatial and/or spatiotemporal pattern formation has been observed in many biological, physiological, chemical, and electro-chemical systems[1–8] governed by the interaction of diffusion and reaction processes. Majority of the studies of pattern formation in chemically reacting systems are of homogeneous systems. Pattern formation in heterogeneous catalytic and electrochemical systems, like wires, pellets, and packed bed reactors has been known for 20 years. Recent reviews of the

Correspondence concerning this article should be addressed to O. Nekhamkina at aermwon@tx.technion.ac.il.

dynamics, and patterns of single catalytic wires, pellets, and reactors have been presented by Luss[9] and Luss and Sheintuch[10] and of electrochemical systems by Kiss and Hudson[11] and Krischer.[12] The current knowledge and understanding about the formation of transversal temperature patterns has been reviewed by Viswanathan et al.[13]

The obtained results are kinetics-dependent[14] and in the present study we focus on kinetics that admits multiple steady state solutions, with one or two stable states (i.e., a non-oscillatory case). Transversal instabilities of planar fronts in reaction-diffusion (RD) systems are known to emerge if the ratio of the diffusion coefficients of the inhibitor to the activator exceeds a certain critical value (an extension of the Turing mechanism[1] for an inhomogeneous steady states). The mechanism of transversal pattern formation in reaction-diffusion-advection (RDA) systems is similar. So, we consider first the relevant studies of the RD system, which was intensively investigated before the RDA systems.

For a thermokinetic homogeneous (noncatalytic, $Le = 1$) reaction-diffusion (RD) system with temperature (T) and concentrations (C_i) as its state variables the diffusive instability was analyzed in a pioneering work of Sivashinsky[15] showing the bifurcation condition to be $k/\rho C_p D_i < 1$, where k and D_i are the thermal conductivity and the species diffusivities, respectively. For an autocatalytic isothermal RD system with cubic kinetics, the critical condition was shown[16,17] to be $D_{act}/D_{inh} < 0.435$, where D_{act} and D_{inh} are the diffusivities of an activator and an inhibitor, respectively. This was verified numerically in a series of studies.[18–23]

For RDA systems, only few studies are available in the literature including our recent analytical study of transversal instability in a PBR[24] (see below), and several numerical studies using either a PBR model[25,26] or an isothermal autocatalytic reactor.[27] We review these results to explain the improved condition derived here. Several analytical results are available for a generic pseudo-homogeneous PBR model that accounts for a single exothermic reaction with Arrhenius kinetics and is described by temperature (T) and limiting species concentration (C) as its state variables. For a 1D system, such kinetics predicts, within an appropriate domain of parameters and proper initial conditions, a stable reaction front propagating with a constant form and a constant velocity (i.e., "frozen" in a moving coordinate).

The maximal temperature rise over the "ideal" front ($\Delta T_m = T_{mx} - T_{in}$, or in the dimensionless form y_m, see notations below) is related to the front velocity (V_f) like[28]:

$$y_m = B\frac{1 - V_f}{1 - LeV_f}, \quad \text{or} \quad V_f = \frac{y_m - B}{Ley_m - B}, \tag{1}$$

where B is the adiabatic temperature rise and Le is the Lewis number (the dimensionless heat capacity, see below). An inspection of Eq. 1 shows that (i) in a stationary front the maximal temperature rise is equal to the adiabatic one, i.e., $y_m = B$, (ii) in a downstream propagating front the velocity V_f (>0) cannot exceed the thermal front velocity $V_{th} = 1/Le$, which corresponds to an infinitely large y_m, (iii) in an upstream propagating front V_f (<0) can formally decrease indefinitely whereas the temperature (y_m) is bounded by a limit value (B/Le) , i.e.,

$$-\infty < V_f < V_{th}, \;\; B/Le < y_m < \infty \tag{2}$$

Note that relations (1 and 2) are valid with any values of axial Pe_T and Pe_C, assuming that conversion at the reactor exit is complete.

To determine y_m and V_f separately, an approximate relation has been derived in Reference 29 and 30 for the limiting case of negligible mass dispersion ($Pe_C \to \infty$), which in the dimensionless form (see below) can be written as following:

$$F(y_m, V_f)E(y_m) = \beta, \tag{3}$$

where

$$F(y_m, V_f) = \frac{Day_m}{BPe_T(1 - V_f)^2}, \;\; E(y_m) = \exp\left(\frac{y_m}{1 + y_m/\gamma}\right), \;\; \beta = \frac{y_m}{(1 + y_m/\gamma)^2} \tag{4}$$

For finite Pe_C this relation was recently extended by us[31] yielding:

$$\log[1 + 2\alpha F(y_m, V_f)E(y_m)] = \frac{2\alpha\beta}{1 + \alpha}, \;\; \alpha = \frac{BPe_T}{y_m Pe_C} \tag{5}$$

The obtained approximation (5) was shown to be in a good agreement with direct simulations results for $Pe_C \gg Pe_T$, whereas the agreement becomes poorer with decreasing the Pe_C/Pe_T ratio.

In our recently published study,[24] we conducted a linear stability analysis of an ideal planar front in a homogeneous thermokinetic model of a PBR and derived an approximate criterion of transversal symmetry breaking to be

$$\alpha > 1 \;\; \text{or} \;\; Pe_{T\perp}/Pe_{C\perp} > y_m/B \tag{6}$$

This condition imposes a restriction on the ratio of the mass to heat transfer coefficients. As for realistic conditions $Pe_{C\perp} > Pe_{T\perp}$ and assuming that the ratio of the mass to heat dispersivities in the axial and transversal directions are equal ($Pe_{C\perp}/Pe_{T\perp} = Pe_C/Pe_T$), condition (6) can be satisfied only in an upstream propagating front ($y_m < B$), and in the case of stationary fronts ($y_m = B$) is reduced to $Pe_C < Pe_T$, which coincides with the bifurcation condition derived for a simplified shallow reactor (RD) model.[32]

Several reported studies focused on numerical analysis of transversal instabilities of planar fronts[25–27]: In one of the first studies of the subject, Balakotaiah et al.[25] using a three-variable (two species and temperature) model with Langmuir-Hinshelwood kinetics, simulated stationary (nonrotating) transversal patterns with

$$Pe_{T\perp}/Pe_{C\perp} > 2$$

Note that this condition is more restrictive than condition (6) and cannot be satisfied for a feasible operating domain.

Direct numerical simulations of a simplified 2D cylindrical shell model[24] for a set of parameters just above the bifurcation condition (6) showed formation of stable nonrotating

transversal patterns on a shell of large radius ($R > L$); with reasonable $R < L$ transversal patterns can be excited but were found to relax to planar fronts after long time.[33] These results suggest to refine the bifurcation condition (6) and to elucidate the role of the reactor radius on the pattern selection. In the present study, we propose a new criterion of transversal instability in PBRs using an alternative approach. This new approach is based on the analysis of the dependence of the velocity of the curvilinear front (V_f^C) on the front curvature (K) using a critical condition for bifurcation

$$\frac{dV_f^C}{dK}|_{K=0} = 0 \tag{7}$$

For that purpose, we derive approximate relations for the propagation velocity and the maximal temperature rise of a curvilinear front in a PBR assuming equal dispersivities of heat and mass in the axial and transversal directions, i.e., $Pe_C = Pe_{C\perp}$, and $Pe_T = Pe_{T\perp}$.

The new criterion and criterion (6) are verified by comparison with the linear stability analysis (LSA) results. The LSA of a numerically obtained 1D front solution allows to formulate the relevant matrix eigenvalue problem and to construct the dispersion curves showing the dependence of the maximal growth rate (σ) on the spatial wave number (k). The limiting (maximal) wave number $k_{\lim}$ with zero eigenvalue allows, in turn, to find the corresponding minimal system width $S_{\lim}$ (in the direction normal to the front propagation or $R_{\lim}$ for a cylindrical shell model), which can sustain transversal perturbations. In systems of sufficiently large S multiwave patterns with the dominant wave length corresponding to fastest growing waves are expected. The transition behavior between a one-wave and a two-wave structures, and similar transitions at higher S are not clear. We have recently found[34] formation of rotating patterns in these transitions for both RDA and RD systems and we pursue this issue in the present study.

The structure of this article is as follows: in the next section we present a 3D PBR model, a 1D planar front solution, the linear stability analysis and derive a criterion of transversal instability of planar fronts. Direct numerical simulation of the 2D cylindrical shell reactor model which is the simplest 2D geometry that can capture both rotating and nonrotating patterns of the 3D model are presented in the third section. We map bifurcation diagrams showing domains of different modes (the generic one- and two-wave "frozen" inhomogeneous front solutions and rigid one-wave rotating patterns in the gaps between them) using the shell radius as a bifurcation parameter. A good agreement between the critical parameters predicted by the LSA and by simulations was obtained. In concluding remarks, we address both the practical and the scientific novelty of the obtained results and also consider a point for future investigation: an extension of the 2D cylindrical shell model results to predict the realistic 3D patterns.

Reactor Model and a Planar Front

Problem statement

We analyze pattern formation for the generic pseudo-homogeneous model of a fixed bed reactor catalyzing a first order reaction of Arrhenius-kinetics. In the adiabatic case assuming noncatalytic reactor walls, the balance equations may be written in the following dimensionless form:

$$\frac{\partial x}{\partial \tau} + \frac{\partial x}{\partial \xi} - \frac{1}{Pe_C}\frac{\partial^2 x}{\partial \xi^2} - \frac{1}{Pe_{C\perp}}\nabla_\perp^2 x = (1-x)f(y) \tag{8}$$

$$Le\frac{\partial y}{\partial \tau} + \frac{\partial y}{\partial \xi} - \frac{1}{Pe_T}\frac{\partial^2 y}{\partial \xi^2} - \frac{1}{Pe_{T\perp}}\nabla_\perp^2 y = B(1-x)f(y), \tag{9}$$

$$f(y) = Da\exp\left(\frac{\gamma y}{\gamma + y}\right) \tag{10}$$

$$\xi = 0, \quad \frac{1}{Pe_C}\frac{\partial x}{\partial \xi} = x, \quad \frac{1}{Pe_T}\frac{\partial y}{\partial \xi} = y, \quad \xi = \bar{L}, \quad \frac{\partial x}{\partial \xi} = 0, \quad \frac{\partial x}{\partial \bar{\xi}} = 0. \tag{11}$$

$$r = 1, \quad \partial x/\partial r = 0, \quad \partial y/\partial r = 0$$

Here, conventional notation is used:

$$x = 1 - \frac{C^k}{C_{\text{in}}^k}, \quad y = \gamma\frac{T - T_{\text{in}}}{T_{\text{in}}}, \quad \xi = \frac{z}{z_0}, \quad \tau = \frac{tu}{z_0}, \quad \tilde{R} = \frac{R}{z_0}$$

$$\gamma = \frac{E_a}{R_g T_{\text{in}}}, \quad \Delta T_{\text{ad}} = \frac{(-\Delta H)C_{\text{in}}^k}{(\rho C_p)_f} \quad B = \gamma\frac{\Delta T_{\text{ad}}}{T_{\text{in}}},$$

$$Da = \frac{z_0}{u}A\exp(-\gamma), \quad Le = \frac{(\rho c_p)_e}{(\rho c_p)_f},$$

$$Pe_T = \frac{(\rho c_p)_f z_0 u}{k_e}, \quad Pe_{T\perp} = Pe_T\frac{k_e}{k_{e\perp}}, \quad Pe_C = \frac{z_0 u}{\varepsilon D_f},$$

$$Pe_{C\perp} = Pe_C\frac{D_f}{D_{f\perp}},$$

Below we consider a case of equal transport coefficients in the axial and transversal directions, i.e., $Pe_{T\perp} = Pe_T$, $Pe_{C\perp} = Pe_C$ (but $Pe_T \neq Pe_C$).

Planar front and its linear stability analysis

The 1D planar front solution is governed by system (8-11) with omitted transversal gradients. Simulations of a sufficiently long region ($L \gg 1$) revealed after a certain transient process formation of a sharp front (the temperature increases from 0.01 y_m up to 0.99 y_m within domain $\Delta\xi \simeq 0.025$) propagating with a constant velocity V_f and a practically "frozen" form $[x_{1D}(\zeta), y_{1D}(\zeta)]$ in a moving coordinate system $\zeta = \xi - V_f\tau$, which obeys:

$$(1 - LeV_f)y_{1D}' - \frac{1}{Pe_T}y_{1D}'' = B(1 - x_{1D})f(y_{1D}) \tag{12}$$

$$(1 - V_f)x_{1D}' - \frac{1}{Pe_C}x_{1D}'' = (1 - x_{1D})f(y_{1D}) \tag{13}$$

The boundary conditions effect becomes insignificant at distance $\zeta \simeq 0.2$ before the front, where the dimensionless temperature and concentrations do not exceed 10^{-8} using BC's (11). So, the simulations in a moving frame were conducted with the Danckwerts BC (11) and we verified, that

the length L is sufficiently long to neglect the BC effect. [Using the Dirichlet conditions ($y(0) = x(0) = 0$) practically leads to the same results but appears to be more stiff and can prevent transversal symmetry breaking].

The linear stability analysis of the planar front with respect to transversal perturbations is conducted in a standard way assuming that the perturbed solution can be presented as

$$x(\zeta,\phi,\tau) = x_{1D}(\zeta) + \tilde{x}(\zeta)e^{\sigma\tau+ik\phi},$$
$$y(\zeta,\phi,\tau) = y_{1D}(\zeta) + \tilde{y}(\zeta)e^{\sigma\tau+ik\phi}, \quad (14)$$

where $\tilde{x}(\zeta)$ and $\tilde{y}(\zeta)$ are small perturbations, σ is the growth rate, and k is the spatial wave number. Such an approach allows to determine in a 2D problem a continuous spectrum of the spatial wave number k for an unbounded (in the transversal direction) planar domain and a critical shell (actually ring) radius corresponding to the first mode ($R^1_{\text{ring}} = 1/k$) for the cylindrical shell model.

Substituting relations (14) into linearized system (8–9) while accounting for Eqs. 12 and 13 we obtain the following system

$$\sigma\tilde{x} = -(1-V_{\text{f}})\tilde{x}' + \frac{1}{Pe_C}\tilde{x}'' + \left(f'_x - \frac{k^2}{Pe_C}\right)\tilde{x} + f'_y\tilde{y} \quad (15)$$

$$Le\sigma\tilde{y} = -(1-LeV_{\text{f}})\tilde{y}' + \frac{1}{Pe_T}\tilde{y}'' + \left(Bf'_y - \frac{k^2}{Pe_T}\right)\tilde{y} + Bf'_x\tilde{x} \quad (16)$$

Equations 15 and 16 using finite-difference approximations of differential operators can be converted for each 1D solution preliminary defined on N spatial points into a ($2N \times 2N$) eigenvalue matrix problem. The latter can be solved numerically yielding the largest eigenvalue σ for each given k . Similar procedure was applied in the previous studies of the RDA[25–27] and RD[18–21] systems.

Criterion of the planar front instability

Assuming that the curvature radius $R_{\text{c}} = 1/K$ (K is the local curvature) is much larger than the front width, one can introduce a local polar coordinate system (ρ, θ) with

$$\frac{\partial}{\partial\zeta^2} = \frac{\partial^2}{\partial\rho^2} + K\frac{\partial}{\partial\rho}$$

Then, the balance Eqs. 12 and 13 may be rewritten in the following form:

$$\left(1 - LeV_{\text{f}} - \frac{K}{Pe_T}\right)y' - \frac{1}{Pe_T}y'' = B(1-x)f(y) \quad (17)$$

$$\left(1 - V_{\text{f}} - \frac{K}{Pe_C}\right)x' - \frac{1}{Pe_C}x'' = (1-x)f(y) \quad (18)$$

where primes denote derivatives with respect to ρ, whereas the boundary conditions for an ''ideal'' front take a form:

$$\rho\to 0, x = 0,\ \ y = 0,\ \ x' = 0,\ \ y' = 0;\ \ \rho\to\infty,\ \ x = 1,$$
$$y = y_{\text{m}},\ \ x' = 0,\ \ y' = 0 \quad (19)$$

Combining Eqs. 17 and 18 results in:

$$\left(1 - LeV_{\text{f}} - \frac{K}{Pe_T}\right)y' - B\left(1 - V_{\text{f}} - \frac{K}{Pe_C}\right)x' - \frac{1}{Pe_T}y'' + \frac{B}{Pe_C}x'' = 0 \quad (20)$$

Integrating this equation while accounting for BC yields:

$$y_{\text{m}} = B\frac{1 - V_{\text{f}} - K/Pe_C}{1 - LeV_{\text{f}} - K/Pe_T} \quad \text{or}$$
$$V_{\text{f}} = \frac{y_{\text{m}}(1 - K/Pe_T) - B(1 - K/Pe_C)}{Ley_{\text{m}} - B}, \quad (21)$$

which differ from the appropriate relations for a planar front (Eq. 1) by additional terms accounting for finite K.

To derive an additional relation between V_{f} and y_{m} we use an approach developed in our study of a planar front characteristics with a finite mass dispersion,[31] which in turn, follows the previous studies of Kiselev and Matros.[29,30] This approach (see Appendix A) results in the following approximate relation:

$$\frac{2\alpha\beta}{1+\alpha} = \log[1 + 2\alpha\tilde{F}(y_m, V_{\text{f}}, K)E(y_{\text{m}})], \quad (22)$$

$$\tilde{F}(y_{\text{m}}, V_{\text{f}}, K) = \frac{Day_{\text{m}}}{BPe_T(1 - V_{\text{f}} - K/Pe_C)^2},$$

where β and $E(y_{\text{m}})$ are defined by relations (4), whereas function $\tilde{F}(y_{\text{m}}, V_{\text{f}}, K)$ is reduced to function $F(y_{\text{m}},V_{\text{f}})$ (4) with $K = 0$. The bifurcation condition of symmetry breaking of a planar front can be formulated as

$$\frac{dV_{\text{f}}}{dK}|_{K=0} = 0 \quad (23)$$

Using the algebraic system composed of the latter of relations (21) and Eq. 22 we obtained (see Appendix B, Eq. 55) the following necessary condition for symmetry breaking:

$$\Phi = \frac{1}{G-1}(1 - \delta - \alpha) > 0, \quad (24)$$

where

$$\delta = G\frac{Pe_T(Ley_{\text{m}} - B)}{Pe_C y_{\text{m}}},$$
$$G = \frac{2F(y_{\text{m}}, V_{\text{f}})E(y_{\text{m}})B}{[1 + 2\alpha F(y_{\text{m}}, V_f)E(y_{\text{m}})](Ley_{\text{m}} - B)C\beta},$$
$$C = -\frac{1}{(1+\alpha)^2} + \frac{1 - y_{\text{m}}/\gamma}{(1+\alpha)(1 + y_{\text{m}}/\gamma)} - \frac{F(y_{\text{m}}, V_{\text{f}})E(y_{\text{m}})}{1 + 2\alpha F(y_{\text{m}}, V_{\text{f}})E(y_{\text{m}})}, \quad (25)$$

Recall that $Ley_{\text{m}} - B > 0$ following conditions (2) and so sgn(G) and sgn(C) coincide. Although we are unable to analyze condition (24) in its general form, several useful observation can be obtained:

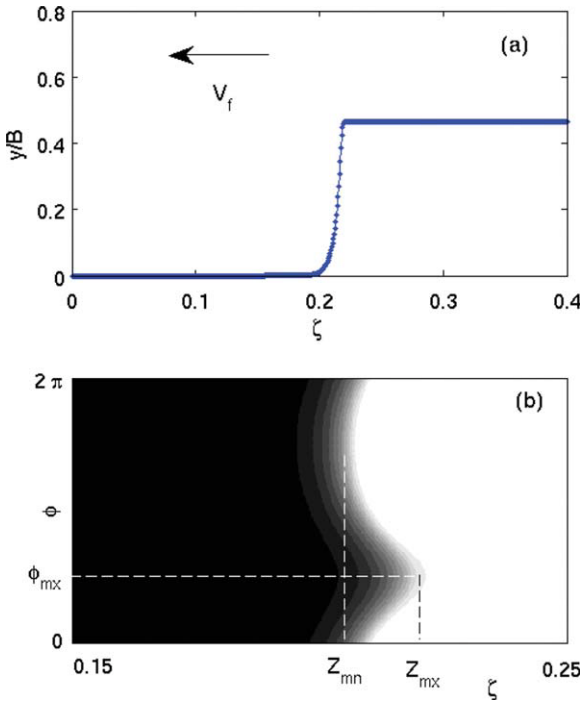

Figure 1. Typical temperature profile in a planar front (a) and a typical 2D "frozen" one-wave pattern showing a snapshot of the temperature on a ζ-fragment of an unfolded cylindrical shell.

Z_{mn} and Z_{mx} mark the minimal and the maximal axial front positions, respectively, ϕ_{mx} is the angular coordinate corresponding to Z_{mx}. [Color figure can be viewed in the online issue, which is available at wileyonlinelibrary.com.]

• In the limiting case with $\alpha \to 0$, ($Pe_C \to \infty$) we have $C < 0$, $G < 0$ and condition (24) cannot be satisfied, i.e., the planar front solution is stable in the case of negligible mass dispersion.

• For moderate α, accounting for $F(y_m,V_f)E(y_m) \gg 1$, expression for C can be reduced to:

$$C \simeq \frac{1}{1+\alpha}\left[\frac{1-y_m/\gamma}{1+y_m/\gamma} - \frac{1}{1+\alpha} - \frac{1+\alpha}{2\alpha}\right]$$

The sum of the last two terms in the square brackets is <1 with $0 < \alpha < 1+\sqrt{2}$ yielding $C < 0$ ($G < 0$). An inspection of Eq. 24 shows that with negative G (and thus, with negative δ) condition $\alpha > 1 + |\delta|$ is sufficient to ensure (24). Thus, we can formulate an approximate sufficient condition for the planar front solution to be unstable with respect to transversal perturbations as:

$$1 + |\delta| < \alpha < 1 + \sqrt{2}. \tag{26}$$

Note, that the lower α-boundary predicted by condition (26) exceeds that, predicted by condition (6). Existence of the upper α-boundary predicted by condition (26) is related with approximations used to estimate a domain of negative G.

Numerical Simulations

We present here the "ideal" (steady in a moving frame) 1D front, the LSA of the 1D solution with respect to transversal perturbations and simulations of the 2D model. The two-dimensional system is a thin annular cylindrical reactor with variation in the flow (axial) and in the azimuthal directions, whereas changes in the radial direction are ignored.

Numerical PDE simulations were conducted for a range of parameters corresponding to upstream propagating fronts following conditions (6) and (24). We use an implicit finite-difference scheme based on an approximate factorization in a moving frame with periodic (each 100 time steps) turning of the front velocity. The 1D simulations were conducted with $L = 0.45$ using a grid with equally spaced 721_z points ($\Delta\zeta = 6.25 \times 10^{-4}$) with the time step $\Delta\tau = 0.001 - 0.02$. The 2D cylindrical shell simulations were conducted with $R = 0-0.03$ using a grid with $721_z \times 101_\phi$ points whereas the convergence was verified on a finer grid.

Predicting the transversal instability

Planar Fronts. 1D system (12, 13) exhibits upstream propagating fronts of the shape shown in Figure 1a; the ratio of the maximal to adiabatic temperature rise is $y_m/B < 1$, following relation (1). With increasing Pe_C, the maximal temperature gradually decreases whereas the front velocity increases (by absolute value) tending to the corresponding asymptotic values with $Pe_C \to \infty$ (Figure 2). Approximation (5) allows to capture these tendencies. The agreement improves for large Pe_C-values, whereas for low $Pe_C \sim$

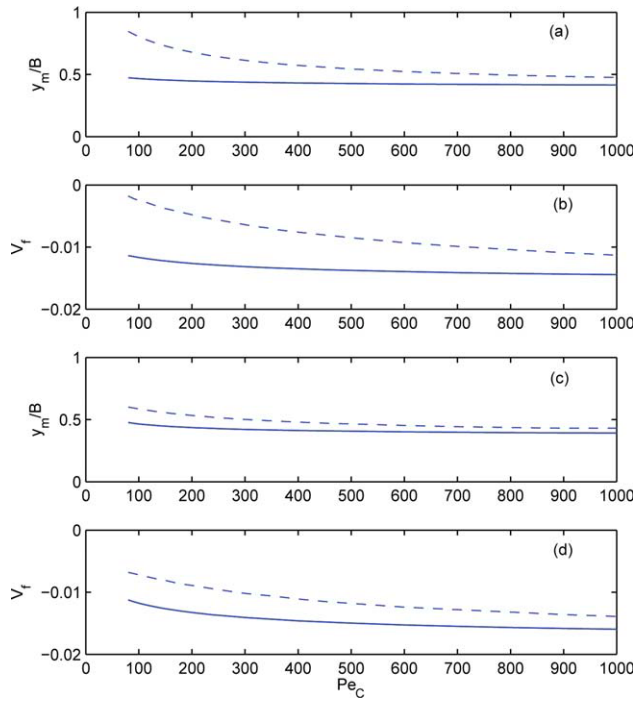

Figure 2. Effect of the mass Peclet number (Pe_C) on the dimensionless temperature rise (y_m/B, a, c) and the velocity (V_f, b, d) of a planar front.

Solid and dashed lines mark numerical simulations (Eqs. 12 and 13) and approximate characteristics (Eqs. 1 and 5), respectively. $Da = 10^{-6}$, $Pe_T = 100$, $Le = 100$; (B, γ): [(100, 50), set 1, plates a, b] and [(200, 30), set 2, plates c, d]. [Color figure can be viewed in the online issue, which is available at wileyonlinelibrary.com.]

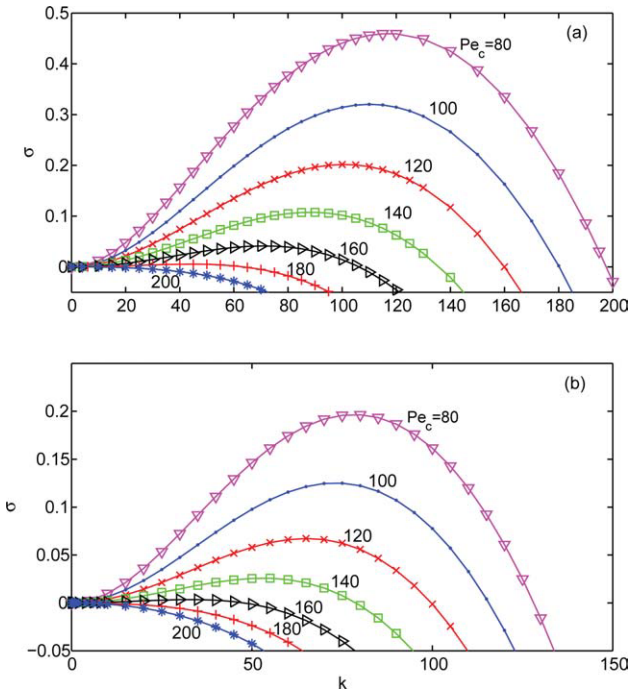

Figure 3. Effect of the mass Peclet number (Pe_C) on the dispersion curves showing the growth rate (σ) dependence on the spatial wave number (k) calculated with the set 1 (a) and set 2 (b) parameters (see Figure 2 caption), respectively.

[Color figure can be viewed in the online issue, which is available at wileyonlinelibrary.com.]

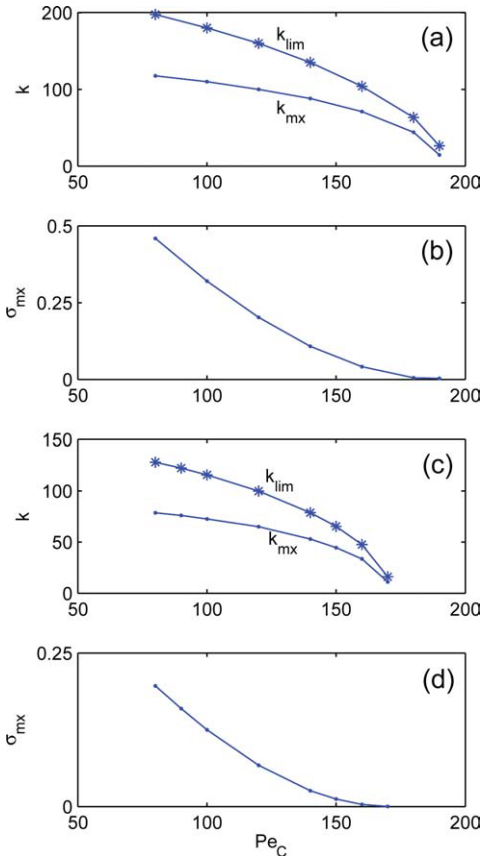

Figure 4. Effect of the mass Peclet number (Pe_C) on the limiting (k_{lim}, a, c, stars) and the maximal (k_{mx}, a, c, dots) wave numbers corresponding to the maximal growth rate (σ_{mx}, b, d) calculated with set 1 (a, b) and set 2 (c, d) parameters (see Figure 2).

[Color figure can be viewed in the online issue, which is available at wileyonlinelibrary.com.]

$O(Pe_T)$ the approximate parameters essentially underestimate the corresponding exact (simulated) values (Figure 2).

Dispersion Relations. Numerical solutions of the eigenvalue matrix problem (15, 16) with preliminary calculated 1D profiles revealed domains of real positive eigenvalues (σ) predicting formation of stationary transversal patterns. Typical dispersion curves calculated for both sets of parameters are shown in Figure 3. The planar front is unstable and admits transversal perturbations within a sufficiently large range of wave numbers k (or reactor radius $R = 1/k$) if the mass Peclet number Pe_C is less than the heat Peclet number Pe_T (see curves with $Pe_C = 80$ in both plates of Figure 3). With increasing Pe_C, the range of unstable wave numbers defined by its upper boundary ($k_{\rm lim}$) gradually shrinks (Figure 4a,c). This is accompanied by monotonous decreasing of the maximal growth rate $\sigma_{\rm mx}$ (Figure 4b,d) and the corresponding wave number $k_{\rm mx}$.

We compare now (Table 1) the Pe_C-boundary of transversally unstable fronts using the linear stability analysis [$(Pe_C^*)_{\rm lin}$] with those calculated using criteria (6) and (24) and referred to as $(Pe_C^*)_\alpha$ and $(Pe_C^*)_{V_f}$, respectively. The former were found to be $\simeq$200 and $\simeq$172 for sets 1 and 2, respectively. Figure 5 illustrates dependence of α and Φ calculated using numerically obtained maximal temperature and front velocities ($y_{\rm m}^{\rm num}$,$V_{\rm f}^{\rm num}$) as functions of Pe_C. The critical numbers $(Pe_C^*)_{V_f}$ predicted using condition (24) (Table 1) are in a good agreement with that following from the linear analysis. The critical $(Pe_C^*)_\alpha$ following criterion (6), leads to essential overestimation of the threshold values.

Complex σ with positive real part were not detected within the whole domain of parameters being considered and suggesting that moving (rotating) patterns do not erase. Numerical simulations reveal, however, their emergence far from the LSA bifurcation.

Table 1. Critical Mass Peclet Numbers Calculated Either By the Numerical LSA [$(Pe_C^*)_{\rm lin}$], or By Nonlinear Curvature Analysis [Criterion (24), $(Pe_C^*)v_f$], or By an Approximate LSA [Criterion (6), $(Pe_C^*)_\alpha$]

Critical Mass Peclet Number	Set I	Set II
$(Pe_C^*)_{\rm lin}$	200	172
$(Pe_C^*)v_f$	200 (116)	190 (146)
$(Pe_C^*)_\alpha$	228 (133)	232 (180)

The two latter are calculated using numerically obtained maximal temperature and front velocity ($y_{\rm m}^{\rm num}$ and $V_{\rm f}^{\rm num}$). Critical parameters calculated with approximate values ($y_{\rm m}$, $V_{\rm f}$, Eqs. 1 and 5) are shown in brackets.

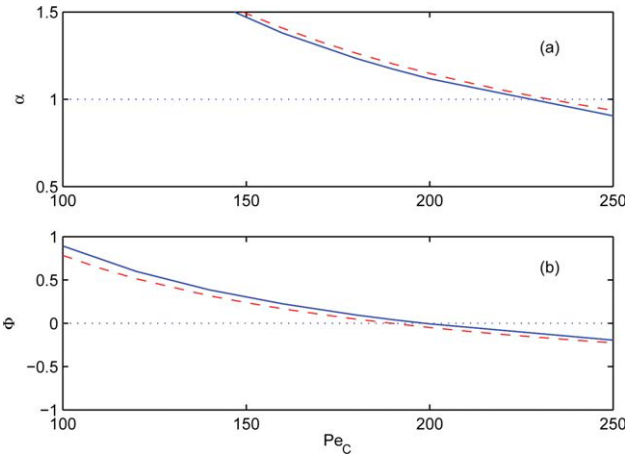

Figure 5. Effect of the mass Peclet number (Pe_C) on the critical parameters that define the transversal instability of a planar front, α (a, Eq. 6), and Φ (b, Eq. 24) for set 1 (solid lines) and set 2 (dashed lines) parameters.

Dotted lines mark the bifurcation conditions $\alpha = 1$ (a) and $\Phi = 0$ (b). [Color figure can be viewed in the online issue, which is available at wileyonlinelibrary.com.]

2D cylindrical shell model

Direct numerical simulations of the 2D shell model aim to verify the linear stability analysis (LSA) predictions of the previous section. We map bifurcation diagrams showing domains of different modes using the shell radius as the bifurcation parameter.

To put our results in perspective we review pertinent results from literature. Effect of the system width (S) in the direction normal to the front propagation was studied with cubic nonlinearity using both the LSA and direct simulations in a 2D domain with no-flux BC in the transversal direction.[16] The authors revealed the existence of stable one-wave and two-wave patterns within certain sub-domains of S. With increasing S further the two-wave patterns lost stability via a supercritical Hopf bifurcation and became oscillatory; various periodic behavior windows were detected including blowup of the period-doubling cascade within certain range of S before a stable three-wave pattern is established. Similar behavior was detected in the gap between the stable three- and four-wave solutions. The corresponding 2D simulations of large planar domains revealed continuous movement of the local extrema of the front position toward the boundaries followed by their arrest and subsequent sharp changes of the wave structure.[16] Using the cylindrical shell model we have recently found for the same kinetics[34] formation of multi-wave "frozen" patterns within appropriate subdomains and rotating waves in the gaps between them for both RDA and RD systems. We extend this study in the present article.

In the present work on the 2D thin cylindrical shell model we found two types of patterns: Propagating transversal fronts "frozen" in an axially moving coordinate and rotating – propagating (i.e., spinning in a laboratory frame) fronts. Simulations were conducted with initial conditions (IC) corresponding to the 1D planar front solutions slightly perturbed in the vicinity of the front. Once a branch of pattern states was obtained for a certain R-domain, it was tracked by gradually increasing/decreasing R.

Nonrotating Patterns. Propagating fronts with a one- and two-wave shape that are "frozen" in a moving, (ζ,ϕ)-frame were simulated for both sets of parameters in Figure 2. To characterize the sustained patterns we traced the front position $[Z_f(\phi,\tau) = \zeta\ (\phi,\tau)]$, defined as the axial coordinate corresponding to a fixed concentration value ($x = 0.5$). Bifurcation diagrams showing (Figure 6) the dependence on R of the longitudinal amplitude of the curvilinear front $[\Delta Z_f(t)$, defined as the difference between the maximal and minimal front positions, Figure 1b] exhibit three domains: one-wave, rotating, and two-wave fronts. To simplify the analysis, we introduced an effective wave number $k_{ef} = 1/(R/m)$, where $m = 1,2$ is the number of transversal waves. The rescaled diagrams plotted in Figures 7 and 8 show that the parameters of the one- and two-wave solutions as functions of k_{ef} practically coincide: The upper k_{ef} boundary of each m-wave subdomain is close to the limiting value k_{lim} predicted by the linear stability analysis conducted in the previous section. The lower k_{ef} boundary is approximately equal to $0.5k_{lim}$, which, in turn, corresponds to the upper k_{ef} limit of the next $(m + 1)$-wave pattern (this was verified for $m = 1$–3, but we did not attempt to trace the three-wave branch further). The amplitudes of the fronts (Figures 7a and 8a) reach the maximal value within the appropriate domains $0.5k_{lim} < k_{ef} < k_{lim}$ and gradually decrease toward the boundaries. The axial front velocities (Figures 7b and 8b) also exhibit nonmonotonic behavior and tend to the corresponding planar front solutions at the edges.

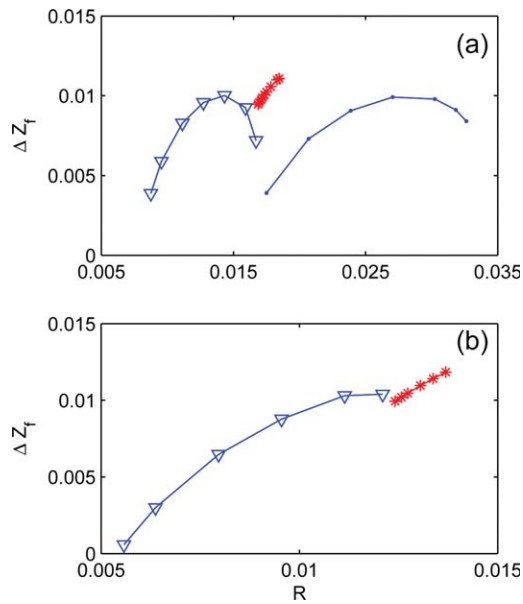

Figure 6. Bifurcation diagram showing the amplitude (ΔZ_f) of stationary one-wave (triangulars), stationary two-wave (dots), and rotating one-wave (stars) solutions as functions of the shell radius (R).

Pe_C =150 (a) and 100 (b). The other parameters of set 1. [Color figure can be viewed in the online issue, which is available at wileyonlinelibrary.com.]

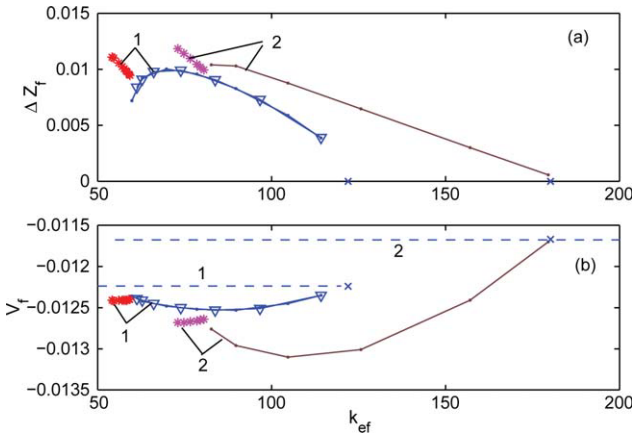

Figure 7. Bifurcation diagram showing the amplitude of transversal patterns (ΔZ_f, a) and the axial front velocity (V_f, b) as functions of the effective wave number k_{ef}.

Crosses mark the limiting points predicted by the linear stability analysis. Pe_C =150 (1) and 100 (2). The other parameters of set 1. Dashed lines in (b) show the planar front velocities. The other notations as in Figure 6. [Color figure can be viewed in the online issue, which is available at wileyonlinelibrary.com.]

Spinning Fronts. Rigid rotating one-wave patterns can emerge in the gap between the "frozen" one- and two-wave solutions. The hot spot behind the convex parts of the fronts rotates and propagates upstream at two different constant velocities (in a laboratory coordinate) forming a spinning

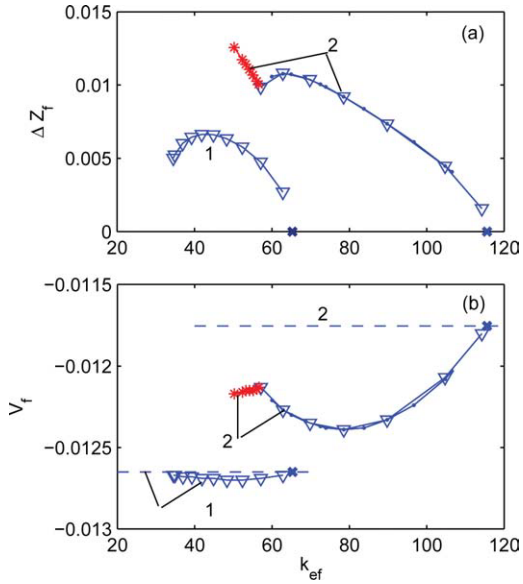

Figure 8. Bifurcation diagram showing the amplitude of transversal patterns (ΔZ_f, a) and the axial front velocity (V_f, b) as functions of the effective wave number k_{ef}.

Crosses mark the limiting points predicted by the linear stability analysis. Pe_C =150 (1) and 100 (2). The other parameters of set 2. Notations as in Figure 7. [Color figure can be viewed in the online issue, which is available at wileyonline library.com.]

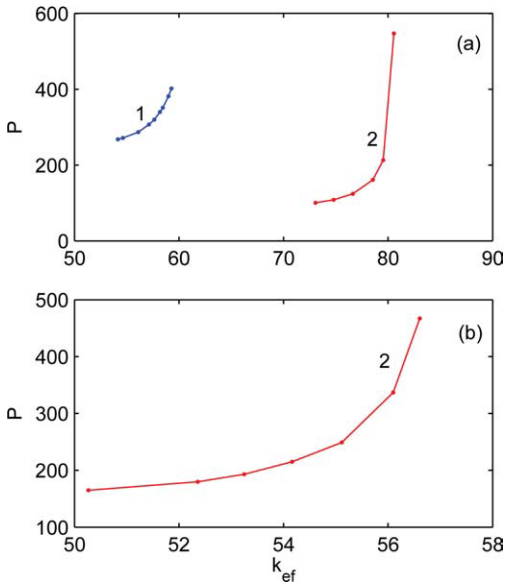

Figure 9. Period of rigid one-wave rotating patterns (P) as a function of the effective wave number k_{ef} for set 1 (a) and set 2 (b) parameters.

Pe_C =150 (1) and 100 (2). [Color figure can be viewed in the online issue, which is available at wileyonlinelibrary.com.]

motion. Such patterns were obtained for set 1 parameters with Pe_C = 100, 150 (Figure 7) and for set 2 parameters with Pe_C = 100 (Figure 8). The rotating front solutions in the middle part of the domain do not depend on the initial conditions, whereas close to the boundaries we found relatively narrow subdomains of coexisting multiple solutions, with their choice depending on IC.

With decreasing R (increasing k), the rotating waves evolve into the one-wave norotating solutions whereas the rotation period exhibits a sharp increase (Figure 9) suggesting a homoclinic bifurcation. With increasing R, rigid rotating patterns are transformed into a one-wave rotating–oscillating pattern. Typical patterns of such a type is illustrated in Figure 10, showing several equally timed front profiles on the unfolded cylindrical shell in the (ζ,ϕ) plane (a) and temporal behavior of the front amplitude (b). The front becomes nonfrozen in the rotating frame and its amplitude exhibits clearly distinguished secondary oscillations (Figure 10b). At the same time, rotation characterized by the angular coordinate of the maximal axial front position ($\phi = \phi_{mx}$, see Figure 1b) occurs at a practically constant angular velocity (Figure 10c), as for rigid rotation. For the case shown in Figure 10, the period of "secondary" oscillations and the rotation period are related approximately as 1:3.5.

Complex Patterns. For even larger R, we find increasing amplitude of the secondary oscillations and formation of rotating patterns with periodic alternation of the one-wave and two-wave structures. Typical transient process leading to formation of complex patterns, using a regular one-wave rotating wave as initial conditions is shown in Figure 11. The initially linear temporal profile $\phi_{mx}(\tau)$ becomes wavy and is gradually transformed into a four step-wise structure (we traced the largest maximum). Such patterns are unstable

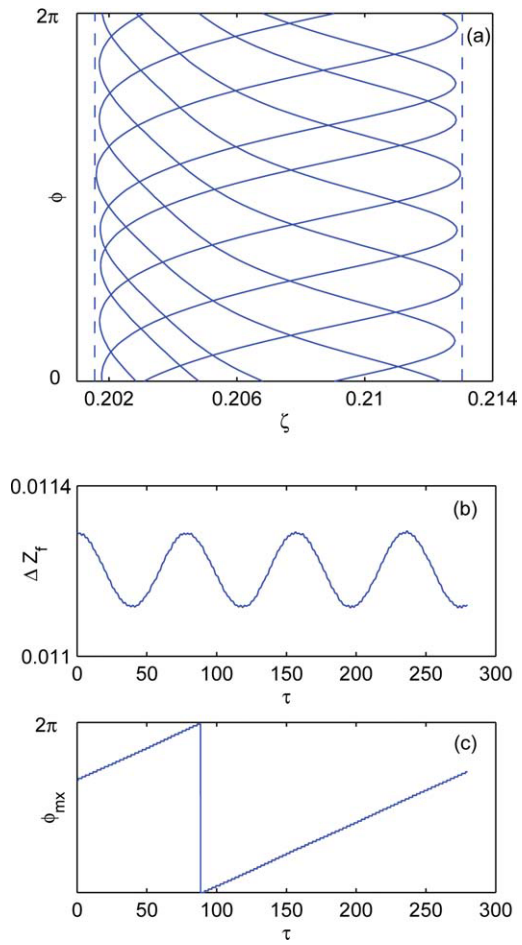

Figure 10. Typical rotating–oscillating one-wave pattern showing several equally timed front profiles on the unfolded cylindrical shell (a), temporal behavior of the front amplitude (ΔZ_f, b), and the angular coordinate of the maximal axial front position (ϕ_{mx}, c).

Dashed lines in plate a mark the minimal and the maximal front positions. $Pe_C = 150$, $R = 0.0185$, other parameters as of set 1. [Color figure can be viewed in the online issue, which is available at wileyonlinelibrary.com.]

and with increasing time converge into nonrotating patterns with periodic (one ↔ two)- wave switching.

Typical complex nonrotating pattern is illustrated in Figure 12 showing one period of the front transformation (in this figure we use an auxiliary axial coordinate $\tilde{\zeta} = \xi - 0.9\langle V_f \rangle \tau$ to shift the front profiles calculated in a frame moving with the average front velocity $\langle V_f \rangle$). At the initial stage (1), the pattern exhibits an asymmetric one-wave front with a narrow concave (in the flow direction) part with $\phi_{mx} \simeq 0.3\pi$ and a wide convex part. With increasing time, the central section of the convex part is retarded and the second valley is formed at $\phi_{mx} \simeq 1.3\pi$. Thus, the two-wave pattern emerges during the phase 2. This pattern is asymmetric as well and with increasing time the largest convex part is retarded, whereas both valleys merge forming a single

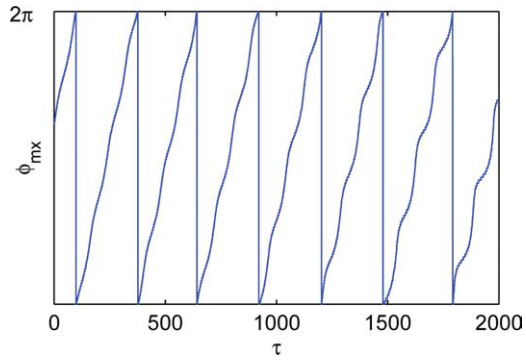

Figure 11. Typical transformation of a one-wave rotating pattern into a complex rotating pattern upon increasing the shell radius showing the temporal behavior of the angular coordinate of the maximal axial front position (ϕ_{mx}).

$Pe_C = 150$, $R = 0.0186$, the other parameters of set 1. [Color figure can be viewed in the online issue, which is available at wileyonlinelibrary.com.]

new valley at $\phi_{mx} \simeq 0.8\pi$. Thus, at stage 3 the pattern exhibits a one-wave structure shifted with respect to the such one of the stage 1 by $\pi/2$. This process is accompanied by oscillatory behavior of the front amplitude (Figure 12b): It

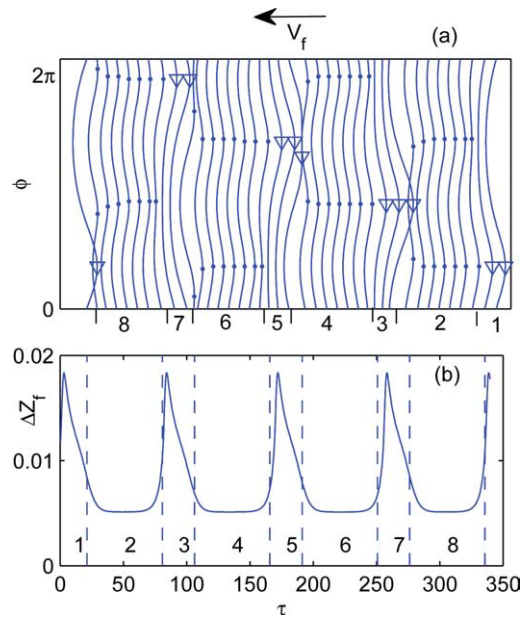

Figure 12. Typical complex nonrotating pattern with a periodic (1 ↔ 2)-wave transformation showing (a) the equally timed ($\Delta\tau$ = 8.5) front profiles on the unfolded cylindrical shell during one period of oscillation and (b) the temporal profile of the front amplitude ΔZ_f.

Odd and even numbered intervals correspond to a one- and two-wave patterns, respectively. Triangulars and dots in plate (a) mark the angular coordinate of the maximal axial front position of one-wave and two-wave patterns. $Pe_C = 100$, $R = 0.0143$, period of oscillations $P \simeq 340$, the other parameters of set 2. [Color figure can be viewed in the online issue, which is available at wileyonlinelibrary.com.]

reaches the maximal value during the one-wave stage and sharply decreases during the two-wave stage. The (one $\leftrightarrow$ two)-wave switching is repeated four times forming a strictly periodic pattern.

With increasing R further, complex patterns with aperiodic alternation of the one-wave and two-wave structures emerge which are finally (with $R \simeq 2/k_{\mathrm{lim}}$) transformed into a frozen two-wave pattern.

Concluding Remarks

In the present work, we obtained a new criterion for transversal instability of planar fronts in reaction-diffusion-advection system with a first-order activated kinetics based on the dependence of the front velocity (V_{f}) on its local curvature (K), using a bifurcation condition $dV_{\mathrm{f}}/dK|_{K=0} = 0$. The derived condition (24) can be satisfied if the ratio of the mass to heat dispersivities do not exceed certain critical value, which agrees with our previous results.[24]

The obtained criterion was verified by the linear stability analysis and by direct two-dimensional simulations of the cylindrical shell model showing a very good agreement of the bifurcation value of the mass Peclet number when numerically calculated values (y_{m},V_{f}) are used in Eq. 24. Using approximate values of the maximal temperature and the front velocity for calculations of the critical Pe_C leads to essential underestimation of this parameter. To explain this result note that the approximate relations for the front velocity accounting for the curvature effect are derived assuming a relatively small mass dispersion. This yields good agreement with $Pe_C/Pe_T \gg 1$ (Figure 2), but transversal instability emerges with the ratio Pe_C/Pe_T around unity.

The engineering implications of this work are the following:

(i) Transversal patterns cannot emerge for the present kinetics in stationary fronts; this is the first rigorous proof of this property for a PBR.

(ii) Transversal patterns can emerge, even if $Pe_C = Pe_T$, in a front moving upstream, provided that the bed diameter is sufficiently large. The minimal required diameter can be predicted by the LSA (Figure 4). The domain of operating conditions shrinks with decreasing Pe_T/Pe_C. As in practice this value varies significantly we cannot make more definite claims.

(iii) These conclusions should be reconsidered for other kinetics. Although we expect similar conclusions for nth order reaction, micro-kinetic bistable model, as in CO oxidation, may induce stationary patterns for $Pe_C = Pe_T$ or even[35] with $Pe_C = 0$. Similar conclusions apply for oscillatory kinetics.[36,37]

(iv) The criterion derived here applies for 3D fixed beds, as we will verify elsewhere by numerical simulations. The linear stability analysis of a 3D model and a cylindrical shell model with respect to transversal perturbations of the form of eigenfunctions [$J_k(\mu_{kn}r)\exp(ik\phi)$ where J_k is the Bessel function of the first kind, μ_{kn} are the transversal eigenvalues which are defined by boundary conditions $dJ_k(\mu_{kn}r)|_{r=0} = 0$[25–27]] is similar to that of the 2D shell model. Thus, the LSA of the (kn)-mode of the 3D model completely coincides with that of the k-mode in the 2D shell model under condition $\mu_{kn} = k^{2D}$.

(v) With increasing R, we expect to find a complex behavior similar to that observed on a plane with the Neumann BC[16] in the transversal direction.

(vi) Although the Lewis number in gas phase catalytic systems is $O(10^3)$, compared with $Le = 100$ used here to simplify construction of the neutral stability curves (the accuracy of the eigenvalue calculations crucially decreases with increasing Le), we expect to find similar patterns for higher Le-values. The results vary qualitatively only for small $Le \sim O(1)$.

The nonlinear-dynamics novelty of this work lies in the simulations of rotating–propagating (spinning) fronts and the structure of operating domains: Beyond the bifurcation threshold we defined in 2D cylindrical shell simulations, sub-domains of stable one- and two-wave frozen (in a moving frame) nonrotating patterns using the shell radius as a bifurcation parameter. The boundaries of these subdomains are in a good agreement with the linear stability analysis results.

Rotating one-wave patterns are shown to emerge in the gap between the one- and two-wave (ζ, ϕ)-"frozen" solutions. Similarly, two-wave rotating patterns can be obtained in the next gap between the two- and three-wave solutions. Such patterns can not be predicted by linear stability analysis of the 1D planar front solution. Nevertheless, similar structure of the oscillatory domain (with rotating waves in the gaps of "frozen" multi-wave solutions) was detected recently by us[34] in the reaction-diffusion (RD) system with a cubic nonlinearity. We have shown[34] that rotating structures emerge in the cylindrical shell model due to periodic boundary conditions and are arrested if the Neumann BC are applied in the transversal direction (in agreement with the previous studies[16]). Similar verification conducted with the RDA model completely approved this observation.

Note, rotating patterns emerge in relatively narrow subdomains which appear to shrink as the bifurcation point following criterion (24) is approached. For example, we obtained rotating waves with the set 2 parameters and $Pe_C = 100$, while with the same parameters and $Pe_C = 150$ such patterns were not detected.

The obtained results allow to get certain insight into pattern formation in the realistic 3D models: Although the shell geometry eliminates the radial gradients, it can be applied to predict the patterns in the 3D case of the form of transversal eigenfunctions $J_k(\mu_{kn}r)\exp(ik\theta)$ which account for both radial and azimuthal gradients [see item (iv) above]. We expect to find (kn)-patterns in the 3D model within domain of radii (R^{3D}) rescaled from the first (one-wave) mode domain of the 2D model (R^{2D}) by $R^{3D} = \mu_{kn}R^{2D}$ at least close to the bifurcation point, and the similar bifurcation structure of the instability domain in the parametric space. This was confirmed by comparison of the direct numerical simulations of the 2D shell and the full 3D model for the case of oscillatory kinetics.[38]

Finally, we note that the obtained rotating, as well as axially-"frozen," patterns were found to emerge in two-variable bistable systems that exhibit ideal fronts in a 1D case, if the ratio of the diffusivities of the inhibitor to the activator exceeds certain critical values. This is contrary to the rotating and nonrotating oscillating patterns in the case of oscillatory kinetics which can emerge[37,38] with $Pe_C \gg Pe_T$, as well as the contrary to spinning mode of gasless combustion

(self-propagating high-temperature synthesis),[39,40] which was revealed for a completely nondiffusive inhibitor under kinetic and thermodynamic conditions corresponding to unstable 1D front propagation.[41,42]

Acknowledgments

This work is supported by Israel-US BSF. O.N. is partially supported by the Center for Absorption in Science, Ministry of Immigrant Absorption State of Israel. M.S. is a member of the Minerva Center of Nonlinear Dynamics and Complex Systems.

Notation

A = rate constant
B = dimensionless exothermicity
c_p = volume-specific heat capacity
C^k = key component concentration
C = parameter defined by Eq. 25
C_p = heat capacity
D = dispersion coefficient
Da = Damkohler number
E_a = activation energy
E = function defined by Eq. 4
f = function defined by Eq. 10
F = function defined by Eq. 4
$\tilde{F}$ = function defined by Eq. 22
g = auxiliary function defined in Appendix A
G = parameter defined by Eq. 25
ΔH = reaction enthalpy
k = perturbation wave number
k_e = effective conductivity
K = curvature
L = reactor length
Le = Lewis number
Pe_T,Pe_C = Peclet numbers of heat- and mass dispersion
p, q = auxiliary functions defined in Appendix A
R = reactor radii
t = time
T = temperature
u = fluid velocities
V_f = front velocity
w = auxiliary variable defined in Appendix A
x = conversion
y = dimensionless temperature
Z = front position

Greek letters

α = parameter defined by Eq. 5
β = parameter defined by Eq. 4
γ = dimensionless activation energy
δ = parameter defined by Eq. 25
ε = porosity
ξ, ζ = dimensionless axial coordinate
ρ = density
ϕ = angular coordinate
Φ = parameter defined by Eq. 24
σ = perturbation growth rate
τ = dimensionless time

Subscripts

ad = adiabatic
e, ef = effective value
f = fluid
in = at the inlet
m = maximal
C = mass
T = temperature
0 = reference value
$\perp$ = transversal

Superscripts

lim = limiting
num = numerical
* = threshold

Literature Cited

1. Turing A. The chemical basis for morphogenesis. *Philos Trans R Soc London B Biol Sci*. 1952;237:37–72.
2. Winfree AT, Strogatz SH. Organizing centers for three-dimensional chemical waves. *Nature*. 1984;311:611–615.
3. Murray JD. *Mathematical Biology*. Berlin: Springer, 1989.
4. Cross M, Hohenberg PC. Pattern formation outside of equilibrium. *Rev Mod Phys*. 1993;65:851–1112.
5. Mikhailov AS, Ertl G. Nonequilibrium structures in condensed systems. *Science*. 1996;272:1596–1597.
6. Kiss IZ, Zhai Y, Hudson JL. Emerging coherence in a population of chemical oscillators. *Science*. 2002;296:1676–1678.
7. Reeves GT, Muratov CB, Schopbach T, Shvartsman SY. Quantitative models of developmental pattern formation. *Dev Cell*. 2006;11:289–300.
8. Tabin CJ. The key to left-right asymmetry. *Cell*. 2006;127:27–32.
9. Luss D. Temperature fronts and patterns in catalytic systems. *Ind Eng Chem Res*. 1997;36:2931–2944.
10. Luss D, Sheintuch M. Spatiotemporal patterns in catalytic systems. *Cat Today*. 2005;105:254–274.
11. Kiss IZ, Hudson JL. Chemical complexity: spontaneous and engineered structures. *AIChE J*. 2003;49:2234–2241.
12. Krischer K. *Nonlinear dynamics in electrochemical systems*. In: Alkire RC, Kolb DM, editors, *Advances in Electrochemical Science and Engineering*. 2003;8:89–208.
13. Viswanathan GA, Sheintuch M, Luss D. Transversal hot zones formation in catalytic packed bed reactors. *Ind Eng Chem Res*. 2008; 47:7509–7523.
14. Merzhanov AG, Rumanov EN. Physics of reaction waves. *Rev of Mod Phys*. 1999;4:1173–1211.
15. Sivashinsky GI. Diffusional-thermal theory of cellular flames. *Combust Sci Technol*. 1977;15:137–146.
16. Horváth D, Petrov V, Scott SK, Showalter K. Instabilities in propagating reaction-diffusion fronts. *J Chem Phys*. 1993;98:6332–6343.
17. Melevanets A, Careta A, Kapral R. Biscale chaos in propagating fronts. *Phys Rev E*. 1995;52:4724–4735.
18. Horváth D, Showalter K. Instabilities in propagating reactiondiffusion fronts of the iodatearsenous acid reaction. *J Chem Phys*. 1995; 102:2471–2478.
19. Toth A, Horváth D, van Saarloos W. Lateral instabilities of cubic autocatalytic reaction fronts in a constant electric field. *J Chem Phys*. 1999;111:10964–10968.
20. Toth A, Horvath D, Jakab E, Merkin JH, Scott SK. Lateral instabilities in cubic autocatalytic reaction fronts: the effect of autocatalyst decay. *J Chem Phys*. 2001;114:9947–9952.
21. Merkin JH, Kiss IZ. Dispersion curves in the diffusional instability of autocatalytic reaction fronts. *Phys Rev E*. 2005;72:026219.
22. D'Hernoncourt J, De Witt A, Merkin JH. Effects of a constant electric field on the diffusional instability of cubic autocatalytic reaction fronts. *J Chem Phys*. 2007;126:104504.
23. Merkin JH. The effects of a complexing agent on the transverse stability of cubic autocatalytic reaction fronts. *J Chem Phys*. 2009;131: 034506.
24. Nekhamkina O, Sheintuch M. Transversal moving-front patterns. Criteria and simulations for two-bed and cylindrical shell packed-bed reactors. *Chem Eng Sci*. 2008;63:3716–3726.
25. Balakotaiah V, Christaforatou EL, West DH. Transverse concentration and temperature non-uniformities in adiabatic packed bed catalytic reactors. *Chem Eng Sci*. 1999;54:1725–1734.
26. Viswanathan GA, Luss D. Hot zones formation and dynamics in long adiabatic packed-bed reactors. *Ind Eng Chem Res*. 2006; 45:7057–7066.
27. Gupta A, Chakraborty S. Linear stability analysis of high- and low-dimensional models for describing mixing-limited pattern formation in homogeneous autocatalytic reactors. *Chem Eng J*. 2009;145:399–411.

28. Wicke E, Vortmeyer D. Zundzonen heterogener reactionen in gasdurchstromten kornerschichten. *Bericht Bunsengesellschaft*. 1959;63: 145–152.
29. Kiselev OV, Matros YuSh. Propagation of the combustion front of a gas mixture in a granular bed of catalyst. *Combust Explos Shock Waves*. 1980;16:152.
30. Kiselev OV. *Theoretical Study of the Phenomena of Heat Waves Movement in Catalytic Bed* (in Russian). Novosibirsk: Russian Academy of Sciences, Institute of Catalysis, 1993.
31. Nekhamkina O, Sheintuch M. Approximate characteristics of a moving temperature front in a fixed-bed catalytic reactor: effect of mass dispersion. *Chem Eng J*. 2009;154:115–119.
32. Viswanathan G, Bindal A, Khinast J, Luss D. Stationary transversal hot zones in adiabatic packed bed reactors. *AIChE J*. 2005;51:3028–3038
33. Nekhamkina O, Sheintuch M. Comments on transversal moving-front patterns. Criteria and simulations for two-bed and cylindrical shell packed-bed reactors by Nekhamkina and Sheintuch. *Chem Eng Sci*. 2009;64:426–427.
34. Nekhamkina O, Sheintuch M. Spinning propagation of diffusionally unstable planar fronts. *Phys Rev E* 2010;81:055204(R).
35. Sheintuch M, Nekhamkina O. Stationary fronts due to weak thermal effects in models of catalytic oxidation. *J Chem Phys*. 2005;123:064708.
36. Digilov R, Nekhamkina O, Sheintuch M. Catalytic spatiotemporal thermal patterns during CO oxidation on cylindrical surfaces: experiments and simulations. *J Chem Phys*. 2006;124:034709.
37. Nekhamkina O, Sheintuch M. Transversal patterns in three-dimensional packed bed reactors: oscillatory kinetics. *AIChE J*. In press.
38. Nekhamkina O, Sheintuch M. Prediction of 3D transversal patterns in packed bed reactors using a reduced 2D model: oscillatory kinetics. In press.
39. Grachev VV, Ivleva TP. Two-dimensional modes of filtration combustion. *Combust Explos Shock Waves*. 1999;35:126–132.
40. Ivleva TP, Merzhanov AG. Structure and variability of spinning reaction waves in three-dimensional excitable media. *Phys Rev E*. 2001;64:036218.
41. Skadinskii KG, Khaikin BI, Merzhanov AG. Propagation of a pulsating exothermic reaction front in the condensed phase. *Fizika Gorenia i Vzruva*. 1971;7:19–28.
42. Sivashinsky G. On spinning propagation of combustion waves. *SIAM J Appl Math*. 1981;40:432–438.

Appendix A: Curvature-Dependence of Front Characteristics

Differentiation of Eq. 18 with respect to ζ yields:

$$(1 - V_f - K/Pe_C)x'' - \frac{1}{Pe_C}x''' = -x'f(y) + (1-x)f'_y y' \quad \text{(A1)}$$

With account for the function $f(y)$ (10) we obtain

$$x'' = \frac{1}{1 - V_f - K/Pe_C}\left[-x'f(y) + \frac{(1-x)f}{(1+y/\gamma)^2}y'\right] + \frac{1}{(1 - V_f - K/Pe_C)Pe_C}x''' \quad \text{(A2)}$$

After substituting Eq. A2 into Eq. 18 while neglecting terms of $O(1/Pe_C^2)$ we find:

$$x'\left[(1 - V_f - K/Pe_C) + \frac{f(y)}{Pe_C(1 - V_f - K/Pe_C)}\right] - y'\frac{(1-x)f(y)}{Pe_C(1 - V_f - K/Pe_C)(1+y/\gamma)^2} = (1-x)f(y) \quad \text{(A3)}$$

Integrating of Eq. 20 while accounting for the first of relations (21) results

$$\frac{B}{Pe_C}x' - \frac{1}{Pe_T}y' = B(1 - V_f - K/Pe_C)\left(x - \frac{y}{y_m}\right) \quad \text{(A4)}$$

Equations A3 and A4 form a linear algebraic system with respect to derivatives x', y' yielding

$$x' \sim \frac{(1-x)f(y)}{Pe_T}\left[1 - \frac{B(x - y/y_m)}{Pe_C/Pe_T(1+y/\gamma)^2}\right] \quad \text{(A5)}$$

$$y' \sim -B(1 - V_f - K/Pe_C)^2(x - y/y_m) \times \left[1 + \frac{f}{Pe_C(1 - V_f - K/Pe_C)^2}\left(1 - \frac{1-x}{x - y/y_m}\right)\right] \quad \text{(A6)}$$

Dividing Eq. A5 by Eq. A6 we obtain a single first-order equation, which after introducing a new variable $w = y/y_m$ can be written in the following form:

$$\frac{dx}{dw} = p(w)g(w,x)q(w,x) \quad \text{(A7)}$$

where

$$p(w) = \frac{y_m f(y_m w)}{BPe_T(1 - V_f - K/Pe_C)^2}, \quad g(w,x) = \frac{1-x}{w-x},$$
$$q(w,x) = \frac{1 - \frac{B(x-w)}{Pe_C/Pe_T(1+y_m w/\gamma)^2}}{1 + \alpha p(w)[1 + g(w,x)]}, \quad \alpha = \frac{BPe_T}{y_m Pe_C} \quad \text{(A8)}$$

The appropriate BC's are:

$$w = 0, \quad x = 0; \quad w = 1, \quad x = 1. \quad \text{(A9)}$$

For the limiting $K \to 0$ case system (A7–A9) is reduced to a problem statement considered previously in Reference 34.

We will briefly describe the following steps. Function $g(w, x)$ has a singularity if $(x, w) \to 1$, however, the limits of $g(w,x)$ and dx/dw are finite:

$$\lim_{w,x\to 1} x'_w = p(1)\frac{-x'_w}{(1-x'_w)}\frac{1}{1 + \alpha p(1)(1 + \frac{-x'_w}{1-x'_w})}$$

Thus,

$$x'_w = \frac{1 + p(1) + \alpha p(1)}{1 + 2\alpha p(1)} \quad \text{(A10)}$$

Now, according to the narrow reaction zone assumption, we can estimate all functions in the RHS of Eq. A7 around $w = 1$: For the function $g(w,x)$ we have:

$$g(w,x) = \frac{1-x}{w-x} \simeq \frac{x'_w}{x'_w - 1} = \frac{1 + p(1)(1+\alpha)}{p(1)(1-\alpha)}$$

or, since $p(1) \gg 1$,

$$g(w,x) = \frac{1+\alpha}{1-\alpha} = \text{const}(w) \quad \text{(A11)}$$

Note, that singularity in $g(w, x)$ with $\alpha \to 1$ will be balanced by function $q(w, x)$: Consider the correction function

$q(w, x, Pe_C)$ (A8) around $w = 1$, while neglecting the term proportional to $(x - w)$ in the numerator:

$$q(w,x) \simeq \frac{1}{1+\alpha p(w)[1+\frac{1+\alpha}{1-\alpha}]} = \frac{1-\alpha}{1-\alpha+2\alpha p(1)} \quad \text{(A12)}$$

Substituting Eqs. A11 and A12 into Eq. A7 we obtain:

$$\frac{dx}{dw} = \frac{(1+\alpha)p(w)}{1-\alpha+2\alpha p(w)} \quad \text{(A13)}$$

Integrating this equation we have:

$$\frac{1}{1+\alpha} = \int_0^1 \frac{p(w)}{1-\alpha+2\alpha p(w)} dw \quad \text{(A14)}$$

Estimating the power of the exponent in $p(w)$ around $w = 1$:

$$\frac{y_m w}{1+y_m w/\gamma} \simeq \frac{y_m}{1+y_m/\gamma} + \beta(w-1), \;\; \beta = \frac{y_m}{(1+y_m/\gamma)^2} \quad \text{(A15)}$$

we obtain

$$\exp\left(\frac{y_m w}{1+y_m w/\gamma}\right) \simeq E(y_m)\exp[\beta(w-1)],$$

and

$$p(w) \simeq \tilde{F}(y_m, V_f, K)E(y_m)\exp[\beta(w-1)] \quad \text{(A16)}$$

where

$$\tilde{F}(y_m, V_f, K) = \frac{Day_m}{BPe_T(1-V_f-K/Pe_C)^2}, \qquad E(y_m) = \exp\left(\frac{y_m}{1+y_m/\gamma}\right) \quad \text{(A17)}$$

Note, that function $\tilde{F}(y_m, V_f, K)$ with $K = 0$ is reduced to function $F(y_m, V_f)$ which is used to define the parameters of a planar front (5). Substituting Eq. A16 in Eq. A14 we get:

$$\frac{1}{1+\alpha} = \tilde{F}(y_m, V_f, K)E(y_m) \times \int_0^1 \frac{\exp[\beta(w-1)]}{1-\alpha+2\alpha\tilde{F}(y_m, V_f, K)E(y_m)\exp[\beta(w-1)]} dw \quad \text{(A18)}$$

Introducing a new variable $v = \exp[\beta(w-1)]$, $dv = v\beta dw$ we obtain

$$\frac{1}{1+\alpha} = \frac{\tilde{F}(y_m, V_f, K)E(y_m)}{\beta} \times \int_{v(0)}^1 \frac{dv}{1-\alpha+2\alpha\tilde{F}(y_m, V_f, K)E(y_m)v} = \frac{1}{2\alpha\beta}\log[1-\alpha+2\alpha\tilde{F}(y_m, V_f, K)E(y_m)v]\Big|_{v(0)}^1 \quad \text{(A19)}$$

Assuming that the value of the logarithm at the lower limit is significantly less than that at the upper limit we obtain

$$\frac{1}{1+\alpha} = \frac{1}{2\alpha\beta}\log\{1+\alpha[2\tilde{F}(y_m, V_f, K)E(y_m)-1]\} \quad \text{(A20)}$$

and with account for $\tilde{F}(y_m, V_f, K)E(y_m) \gg 1$ we finally get

$$\frac{2\alpha\beta}{1+\alpha} = \log[1+2\alpha\tilde{F}(y_m, V_f, K)E(y_m)] \quad \text{(A21)}$$

Appendix B: Bifurcation Condition

After differentiation of the latter of relations (21) with respect to K we obtain (below the prime denotes derivatives with respect to K at $K = 0$):

$$\left.\frac{dV_f}{dK}\right|_{K=0} = \frac{y_m' B(Le-1) + (Ley_m - B)y_m(\alpha-1)/Pe_T}{(Ley_m - B)^2}, \quad \text{(B1)}$$

To simplify the following rearrangement we use the following auxiliary relations [the arguments of functions $F(y_m, V_f)$ and $E(y_m)$ are skipped]:

$$\alpha' = -\alpha\frac{y_m'}{y_m}, \;\; \beta' = \beta y_m' \frac{1-y_m/\gamma}{y_m(1+y_m/\gamma)}, \;\; E' = E\beta\frac{y_m'}{y_m},$$
$$\tilde{F}'(y_m, V_f, K)|_{K=0} = F(y_m, V_f)\left(\frac{y_m'}{y_m} + 2\frac{V_f' + 1/Pe_C}{1-V_f}\right)$$

Accounting for these relations the derivative of the LHS of Eq. 22 is

$$\text{LHS}' = 2\frac{(\alpha'\beta+\alpha\beta')(1+\alpha)-\alpha\beta\alpha'}{(1+\alpha)^2} = \frac{2\alpha\beta}{(1+\alpha)^2}\frac{y_m'}{y_m}\left[-1+(1+\alpha)\frac{1-y_m/\gamma}{1+y_m/\gamma}\right] \quad \text{(B2)}$$

For RHS of Eq. 22 we have:

$$\text{RHS}' = \frac{2}{1+2\alpha FE}(\alpha' FE + \alpha F'E + \alpha FE') = \frac{2\alpha FE}{1+2\alpha FE}\left(-\frac{y_m'}{y_m} + \frac{y_m'}{y_m} + 2\frac{V_f' + 1/Pe_C}{1-V_f} + \beta\frac{y_m'}{y_m}\right) \quad \text{(B3)}$$

Combining Eqs. B2 and B3 we obtain:

$$\beta\frac{y_m'}{y_m}\left[-\frac{1}{(1+\alpha)^2} + \frac{1-y_m/\gamma}{(1+\alpha)(1+y_m/\gamma)} - \frac{FE}{1+2\alpha FE}\right] = \frac{2FE}{(1+2\alpha FE)}\frac{V_f' + 1/Pe_C}{1-V_f} \quad \text{(B4)}$$

Following relations (21)

$$1 - V_f|_{K=0} = \frac{y_m(Le-1)}{Ley_m - B}$$

Substituting the latter into Eq. B4 we obtain

$$y_m' = \frac{2FE}{(1+2\alpha FE)}\frac{(Ley_m - B)}{(Le-1)}\frac{(V_f' + 1/Pe_C)}{C\beta} \quad \text{(B5)}$$

where

$$C = -\frac{1}{(1+\alpha)^2} + \frac{1 - y_m/\gamma}{(1+\alpha)(1+y_m/\gamma)} - \frac{FE}{1+2\alpha FE} \quad \text{(B6)}$$

Substituting Eq. B5 into Eq. B1 we get

$$V_f'(G-1) = \frac{(1-\alpha)y_m}{Pe_T(Ley_m - B)} - \frac{G}{Pe_C}$$

where

$$G = \frac{2F(y_m, V_f)E(y_m)B}{(1+2\alpha F(y_m, V_f)E(y_m))(Ley_m - B)C\beta}$$

Thus, the necessary condition of the transversal instability is:

$$C^* = \frac{1}{G-1}\left[\frac{(1-\alpha)y_m}{Pe_T(Ley_m - B)} - \frac{G}{Pe_C}\right] > 0 \quad \text{(B7)}$$

or

$$\Phi = \frac{1}{G-1}(1-\delta-\alpha) > 0, \quad \delta = G\frac{Pe_T(Ley_m - B)}{Pe_C y_m} \quad \text{(B8)}$$

Recall that $Ley_m - B > 0$ following conditions (2) and so sgn(δ) and sgn(C) coincide.

Manuscript received Mar. 21, 2010, and revision received May 4, 2010.